Airglow measurements of mesospheric wave structures and thermal gradient variability over a low-latitude Indian station

A. Taori*

National Atmospheric Research Laboratory, Pakala Mandal, Gadanki 517 112, India

Simultaneous mesospheric OH and O_2 temperature estimates are used in the present study to characterize the wave perturbations over Gadanki (13.5°N, 79.2°E), a low-latitude station in India. The 65° zenith angle scanning measurements show large variations from one direction to another. The zonal and vertical wavelengths of the observed wave perturbation are found to vary from 740 to 4500 km and 26 to 38 km. The temperature gradient between OH and O_2 layers has been calculated, which shows significant short-period variability. The temperature gradient measurements show large changes from one direction to another. The occurrence of such large temperature gradients within 400 km suggests thermal state of the upper mesosphere to be highly dynamic, which can severely impact the upward propagation of short-period gravity waves.

Keywords: Airglow measurements, mesosphere, temperature, thermal gradient, wave perturbations.

IN spite of the recent progress made in understanding the mesosphere physics, prediction and characterization of mesospheric phenomena remain challenging due to the lack of measurement tools capable of providing continuous information on the thermodynamical parameters[1]. The gravity wave and tides, generated in the lower atmosphere, pass through the mesosphere whose thermodynamical state defines the upward propagation of these waves[2]. This in turn plays a crucial role in determining the neutral–ion coupling[3], which has far-reaching consequences in the processes occurring in thermosphere–ionosphere system[4–6]. The upward propagating waves undergo convective as well as dynamical instability processes and some of them get ducted or become evanescent at mesospheric altitudes[2,7]. While the phase velocity and horizontal scales of the wave perturbation are the important factors for its upward propagation, the ducting of these waves categorizes their horizontal propagation. The duct can either be Doppler duct or thermal duct. Doppler duct arises due to wind–wave interaction, whereas thermal duct depends on the variations in the frequency of natural oscillation which is a function of temperature gradient. The information on the temperature gradient (and thus frequency of natural oscillation) is usually obtained either by space-borne methods[8,9] or ground-based Rayleigh lidars[10]. While the former methods provide a snapshot information, the latter ones provide information generally up to 75 km (unless they use resonant scattering methods such as sodium or potassium lidars[11]) with a time resolution no better than 0.5 h. In this regard, it is worth noting that optical airglow monitoring offers a temporal resolution better than 2 min to study the upper mesospheric temperature variability[6,12–15]. However, efforts to study the temperature gradient using the airglow methods have so far been limited to suggesting the temperature differences between OH and O_2 emission altitudes[16]. We believe that an attempt in this direction may provide a useful tool to understand the modes of variability in the upper mesospheric thermal structure.

In the present study, we propose to use simultaneous OH and O_2 temperature measurements to study the layer-averaged temperature gradient and the short-period variability in the thermal gradient. Further, scanning measurements are performed in the east, west, north and south directions to study the horizontal and vertical wavelengths of the nocturnal wave and variations in the temperature gradient.

Experimental details

We use narrow field-of-view, ground-based photometric measurements of night airglow emissions and space-borne remote sensing instruments. Descriptions of both these methods are as follows.

Ground-based measurements

The nightglow observations were carried out using the mesosphere lower thermosphere photometer (MLTP). The MLTP has 4° full field-of-view and a Hamamatsu H7421-50 photomultiplier tube (PMT) as the detector. It monitors: (a) 840 and 846 nm rotational lines of OH (6–2) band emission, (b) 866 and 868 nm rotational lines of O_2 (0–1) band emission, (c) O(^{1}S) 558 nm emission line and (d) O(^{1}D) 630 nm emission line near simultaneously.

*e-mail: alok.taori@gmail.com

The filters have 0.45 nm full width at half maximum with transmission ~ 50% and are mounted in a temperature-controlled filter wheel. The motion of the filter wheel and PMT counting (counter, C8855-01) are synchronized, and as the filter moves in the optical path of the instrument, data are collected for 10 sec. By doing this for each filter and taking account of the slow movement of the stepper motor, cadence time turns out to be about ~ 90 sec. The derived temperatures have a precision better than 2%. Details of MLTP and validation of the first results are discussed elsewhere[17].

For the present study, the mirror scanning capability of MLTP has been used. In this, after the measurements at zenith, scanning is performed in the east, west, north and south directions at a fixed 65° solar zenith angle (i.e. 35° off-zenith) at both the OH and O_2 emission lines. The 65° zenith angle at 87 km (peak emission altitude of OH emission) corresponds to ~ 186 km horizontal separation, whereas at 94 km (peak emission altitude of O_2 emission) it would correspond to ~ 201 km separation. The mirror scanning motion is synchronized with the filter rotation and counting unit operations. For 10 sec integration at every wavelength of interest in each direction, the resultant repeating time (cadence) of ~ 6 min is achieved. In this article, we present the results of scanning measurements performed on three nights in April 2010 when cloud-free sky prevailed throughout the night, providing an opportunity to retrieve meaningful information on the wave propagation in the collected data.

TIMED–SABER measurements

The sounding of the atmosphere using broadband emission radiometry (SABER), on-board the thermosphere ionosphere mesosphere energetic and dynamics (TIMED) satellite, is a high-precision broadband radiometer which measures limb radiance (at 74°) of the terrestrial atmosphere in 10 selected spectral bands ranging from 1.27 to 15 μm. The temperature values are retrieved from SABER measurements of the atmospheric 15 μm CO_2 limb emission. We use the SABER 1.07 data which have good temperature precision with error in the order of ± 1.4 K in the lower stratosphere, ± 1 K in the middle stratosphere and ± 2 K in the upper stratosphere and lower mesosphere[18]. For the best correspondence with the ground-based MLTP measurements, near-coincident SABER version 1.07 temperatures measurements in a 5° × 5° latitude, longitude grid around Gadanki (13.5°N, 79.2°E) are used in the present study to cross-check and validate our results.

Observations and results

MLTP measurements

The scanning measurements at OH and O_2 emission wavelengths, carried out on 12 and 13 April, 15 and 16 April as well as 19 and 20 April 2010 were used because clear sky conditions persisted for long duration. Details of the observed features are elaborated in the following.

To elaborate the observed oscillatory features in the OH data, Figure 1 plots the night-time temperature variability observed on 15 and 16 April 2010. The presence of a long-period oscillation is noteworthy in all directions. During this night, temperature values ranged from 185 to 210 K in all directions. Together with long-period features, data also reveal large amplitudes of shorter period oscillations. The simple cosine best-fit model[19] is also plotted in the figure (solid red curves), which reveals the wave periods in all the directions to be 10.3 ± 1.9 h. The minimum in phases occurred at 23.75, 23.5 and 23.4 h IST at 65°E, Zenith and 65°W directions with respective peak-to-peak wave amplitudes ~ 18, 18 and 20 K. Similarly, 65°N, zenith and 65°S observations revealed their respective peak-to-peak amplitudes to be ~ 17, 18 and 16 K.

The O_2 temperature variability (Figure 2) on this night shows very small amplitudes of long-period oscillatory features (except at 65°E). Similar to the OH data, O_2 data were also subjected to best-fitting analysis. Unlike the OH data, O_2 data show dominance of short-period oscillations over the long-period feature. The O_2 temperatures range from 175 to 195 K on this night. The peak-to-peak amplitudes are noted to be ~ 3 K at 65°E with minima of phase at 21 h IST.

Assuming the centroid of OH and O_2 emission layers to remain at 87 and 94 km, the observed temperature differences can be converted into the temperature gradients (temperature gradient = temperature difference/altitude difference). These calculated temperature gradients are plotted in Figure 3. During this night, the temperature gradient is negative throughout, which indicates that the mesopause was situated ≥ 94 km. It can be noted that there exist significant differences from one direction to another together with large oscillatory features in the observed night temperature gradient variability.

It is clearly noted that OH and O_2 temperature data indicate the presence of short-period features having large amplitudes. To identify the dominant wave periods in the data, we carried out Lomb–Scargle periodogram (LSP) analysis. The results of the LSP analysis of the above elaborated observations are shown in Figure 4, where the top panel represents O_2 data, the middle panel is for OH data, and the bottom panel plots the LSP analysis on the deduced temperature gradients. Dashed horizontal lines in each plot indicate the 90% confidence level. The shorter period waves are found to have larger amplitudes in O_2 data. It is noted that in spite of the commonality in observed wave periods, there exist large differences in amplitudes from one direction to another. The OH data, on the other hand, reveal long-period oscillations to be the most significant. The LSP analysis clearly indicates that OH data, in all the directions, were dominated by

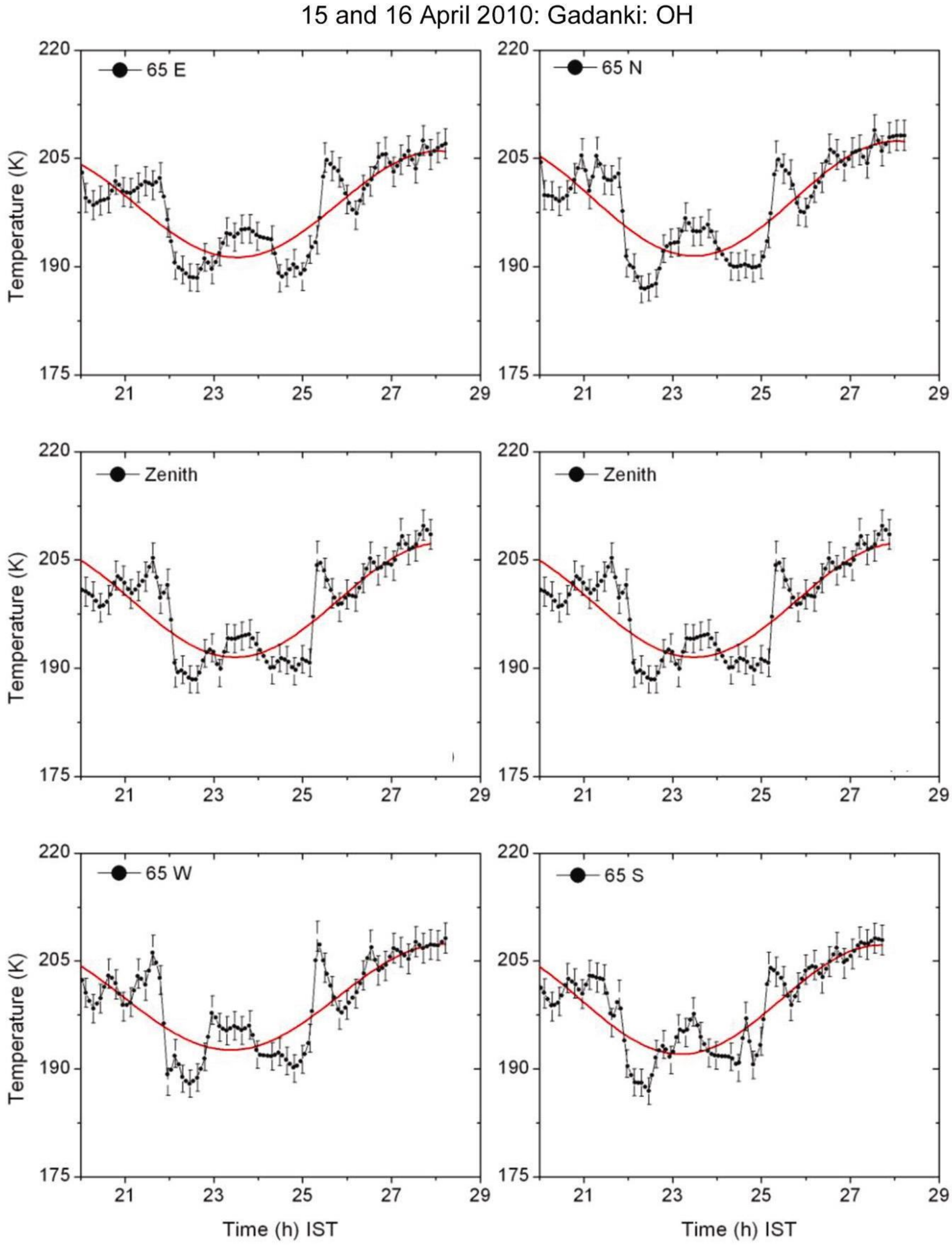

Figure 1. Temperature variability noted in OH data on 15 and 16 April 2010. Red curves show the results of best-fit cosine model. Vertical bars with each data point show errors in the temperature estimates. Large spatio-temporal variations are noteworthy.

8–10 h wave period, which was earlier revealed in the best-fit analysis. Waves with periods ~ 1.2, 2.3 and 3.5 h were also found to have dominant amplitudes in the OH data. The temperature gradient also reveals an 8–10 h wave period to have the largest amplitude in data with significant amplitudes at 1 and 2.5 h periods. The differences of periodogram in short (≤ 2 h) periods among different directions are noteworthy.

Similar to the analysis carried out for 15 and 16 April 2010 (as explained above), 12 and 13 April as well as 19 and 20 April 2010 data were subjected to the best-fit and LSP analyses. Results of best-fit analysis are shown in Table 1. The LSP analysis corresponding to 12 and 13 April 2010 data is shown in Figure 5. Top, middle and bottom panels of the figure plot the LSP results for O_2 data, OH data and deduced temperature gradients. It is clear that 6–8 h wave was dominant in the data followed by small-period waves commonly noted in both OH and O_2 temperatures as well as in temperature gradient variability. Note that dashed horizontal lines in each plot represent 90% significance levels. Figure 6 plots the results of LSP analysis corresponding to 19 and 20 April 2010.

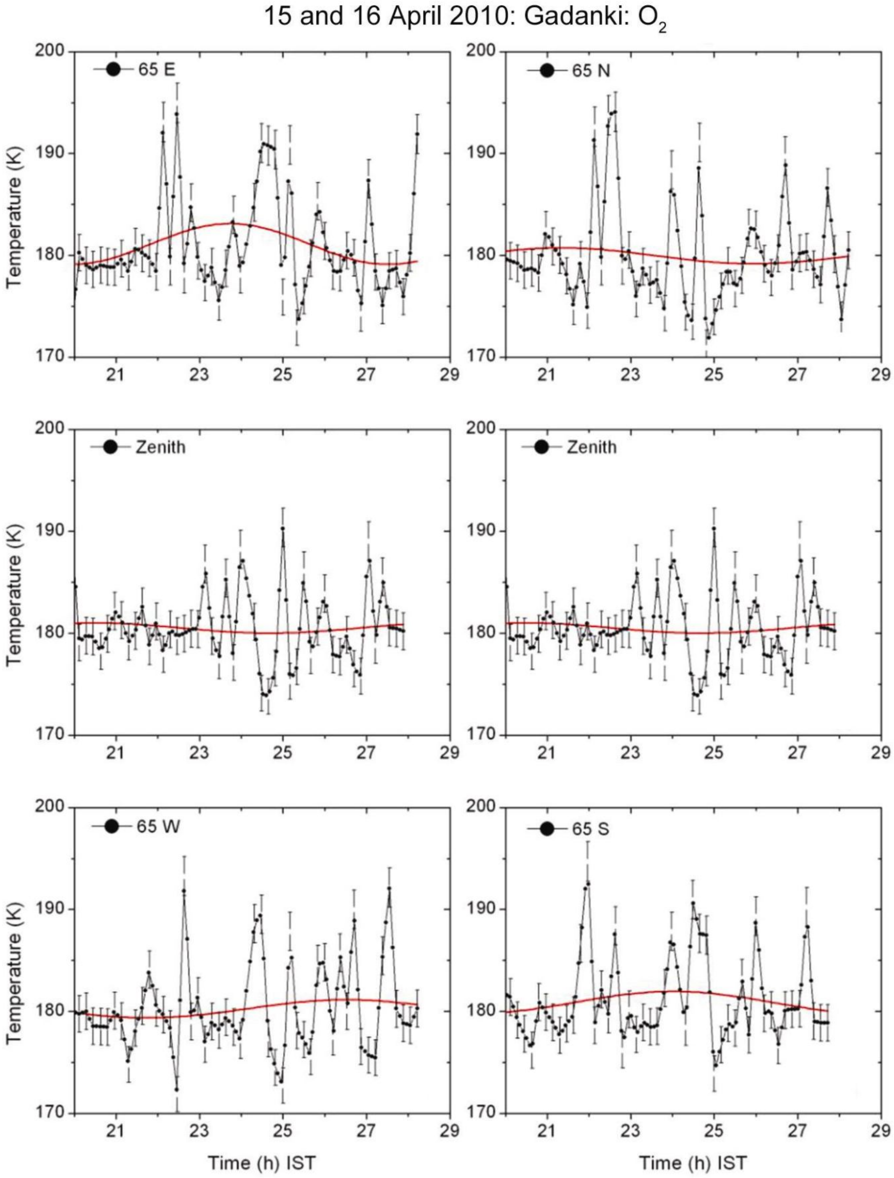

Figure 2. O_2 layer temperature variability on 15 and 16 April 2010. Red curves show the results of best-fit cosine model. Large changes in the wave signatures from one direction to another are noteworthy. It is evident from the plot that short-period wave structures have larger amplitudes compared to the long-period wave structures.

Unlike other nights where a long-period wave was found to dominate the nocturnal variability, during this night 3–6 h wave was dominant. One may also note that OH data show 4–6 h wave periods as principal component, whereas at O_2 altitudes, significantly small period, i.e. 3–4 h waves are prominent. Temperature gradients show 4–5 h, 3 h and smaller periods to have significant amplitudes.

SABER measurements

The SABER data, corresponding to the MLTP observations carried out on 12 and 13 April, 15 and 16 April as well as 19 and 20 April 2010 are shown in Figure 7. Individual profiles show the SABER temperature estimates corresponding to a 5° × 5° latitude, longitude grid around Gadanki (13.5°N, 79.2°E) for best coincidence with the night airglow measurements. Open circles show the SABER values, and solid green lines exhibit 5 km Gaussian averaging on them (to compare the values with airglow OH and O_2 layers which have a skewed Gaussian profile with ~ 8 km thickness). Figure 7 *a* and *b* shows the temperature variability observed on 12 and 13 April 2010. During this night only two SABER passes were available in the selected spatial and temporal grid. The presence of large thermal inversion at ~ 85 km is evident

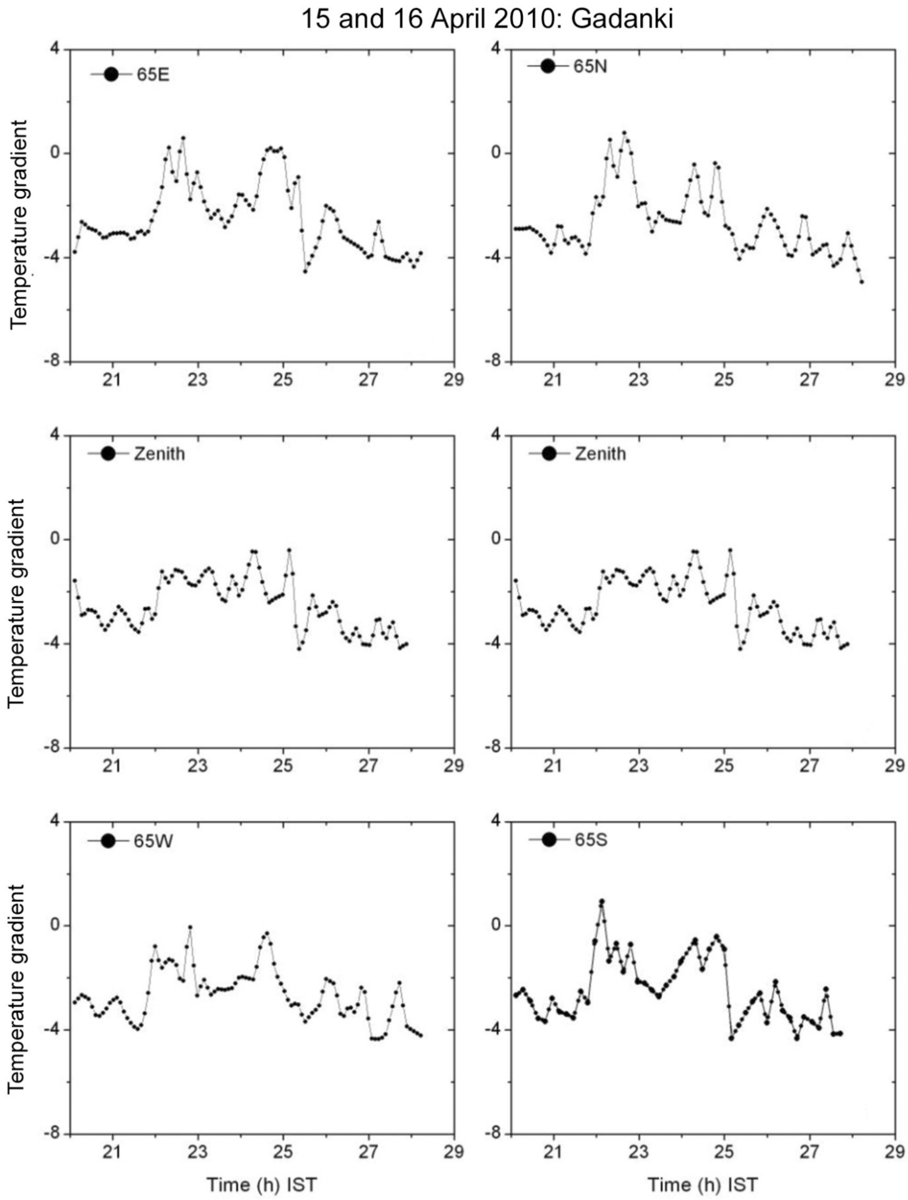

Figure 3. Deduced temperature gradient variability using OH and O_2 temperature data on 15 and 16 April 2010. Large variability in temporal as well as in different directions is noteworthy.

Table 1. Quality of wave fitting (using χ^2 analysis) and summary of long-period nocturnal wave characteristics noted during the period of observation

		Goodness of fit (χ^2)				
Date	Wave period (h)	OH East, west, zenith, north, south	O_2 East, west, zenith, north, south	Zonal wavelength (km)	Meridional wavelength (km)	Vertical wavelength (km)
12 and 13 April 2010	7.1 ± 1.2	0.81, 0.61, 0.71, 0.74, 0.63	0.61, 0.21, 0.25, 0.62, 0.34	746 ± 72	1250 ± 190	28.2 ± 4
15 and 16 April 2010	10.3 ± 1.9	0.88, 0.89, 0.91, 0.87, 0.91	0.52, 0.22, 0.28, 0.24, 0.26	3600 ± 1230	4505 ± 780	26.2 ± 5
19 and 20 April 2010	4.1 ± 0.9	0.85, 0.64, 0.8, 0.83, 0.61	0.56, 0.34, 0.29, 0.52, 0.28	1200 ± 300	990 ± 200	38 ± 5.2

over Gadanki (13.5°N) as well as in the north latitudes (15.6°N). On 15 and 16 April 2010, three SABER passes were available and corresponding data are plotted in Figure 7*c–e*. On this night also similar to earlier nights, large temperature inversion is noted. However, the minima of temperature on this night occur at ~100 km, unlike at ~80 km noted on earlier nights. Large latitudinal variations in the thermal structures are also evident in the temperature profiles. There were three passes of SABER over the selected spatial grid corresponding to the night of 19 and 20 April 2010 (Figure 7*f–h*). Multiple temperature inversions were found to occur at 70–100 km altitudes. The temperature inversions that occurred at 26:50 h (i.e. 2.8 h IST) between 80 and 95 km were found to be either very small (Figure 7*g*) or absent (Figure 7*f*) in the post-evening hours.

Discussion

Observations clearly exhibit wave structures in the temperature data which also show large variability from one direction to another. These thermal structures had large amplitudes in OH layer altitudes compared to O_2. On the other hand, O_2 data show short-period structures (<2 h wave-period) having larger amplitudes. First, the structure of dominant nocturnal wave in OH and O_2 data is studied. Further, the large variability observed in

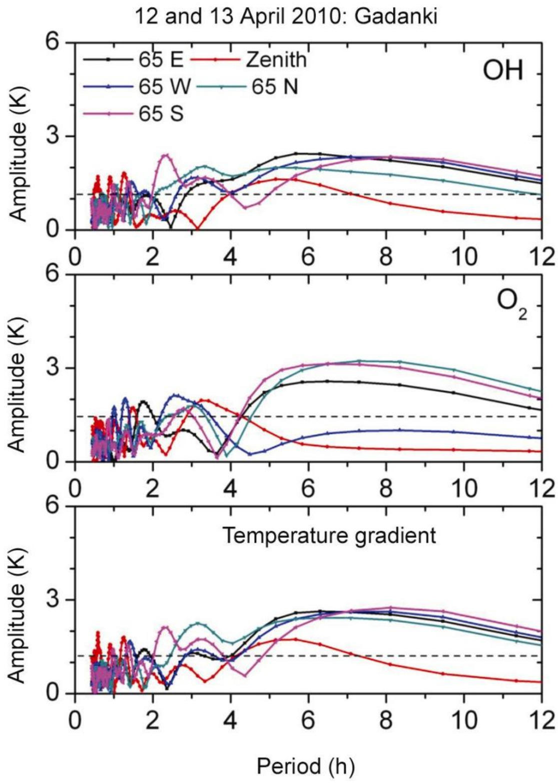

Figure 5. Same as Figure 4, but for the night airglow measurements carried out on 12 and 13 April 2010.

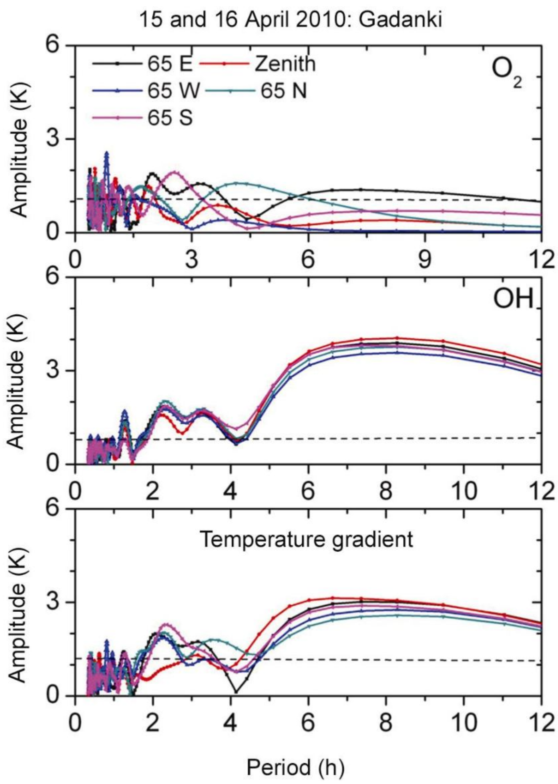

Figure 4. Lomb–Scargle periodogram analysis for the data corresponding to 15 and 16 April 2010 and shown in Figures 1–3.

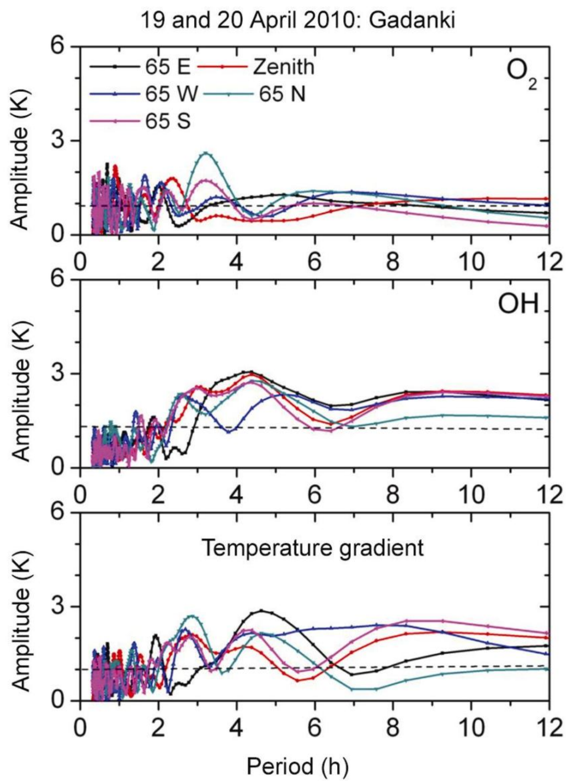

Figure 6. Same as Figure 4, but for the night airglow measurements carried out on 19 and 20 April 2010.

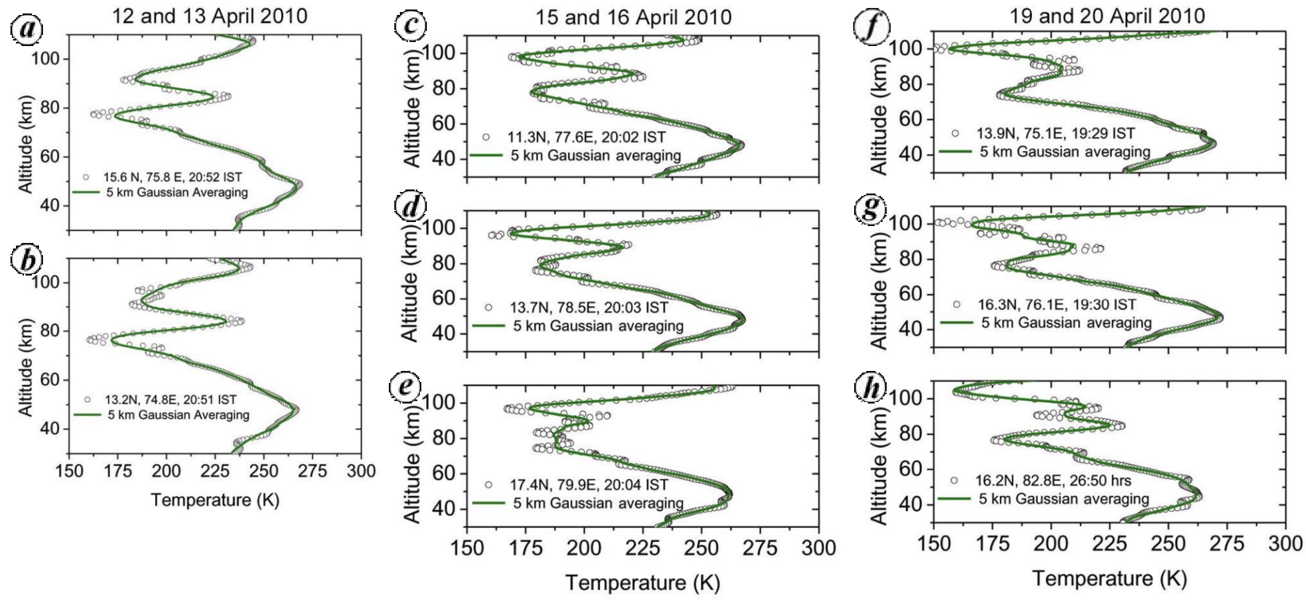

Figure 7. Available TIMED–SABER passes nearby Gadanki (13.5 N, 79.2 E) in a 5° × 5° grid. The open black circles in each plot are actual measurements, while the solid green lines represent a 5 km Gaussian averaged data.

the temperature gradients is elaborated and deduced temperature gradients are compared with the SABER observed temperature values.

Wave characteristics

It is important to note that the O_2 data show long-period wave amplitudes to be much smaller, while the short-period features dominate. This may happen because of long-period waves getting dissipated while approaching the O_2 layer. This leads to the breaking of waves and secondary wave generation enhancing the amplitudes of the short-period wave spectrum. For example, on 15 and 16 April, in the O_2 data long-period wave was noted only in the east direction, while in other directions the amplitude of long-period wave was negligible, which indicates the dissipation of waves at preferential direction, possibly because of background dynamical conditions such as wind-induced filtering. A detailed discussion on this aspect is beyond the scope of the present study. As explained earlier, the simple cosine best-fit analysis provides amplitude and phase of the wave perturbation which are dominant on a given night. This information is used to study wave characteristics. Also, the 65° zenith angle corresponds to ~ 186 km at 87 km and ~ 201 km at 94 km altitudes. It is noteworthy that the dominant nocturnal waves in the data are found to be 7.1 ± 1.2 h, 10.9 ± 1.9 h and 4.1 ± 0.9 h on 12 and 13 April, 15 and 16 April as well as 19 and 20 April 2010 respectively. It can be clearly noted in Figure 1, and as revealed by the best-fit analysis of OH data, that minima of phase in zonal direction, i.e. 65°E, zenith and 65°W, occurred at 24.1, 23.25 and 23 h respectively. This results in zonal propagation velocity of ~ 338 km/h. The period of this wave was 10.9 h, therefore, the horizontal wavelength of this wave is estimated to be ~ 3686 km. In meridional direction, the minima of phase is noted to occur at 23.9 h in the north to 23 h in the south, resulting in horizontal wavelength of ~ 4505 km. To obtain the vertical wavelength of the wave, we use O_2 data corresponding to 65° east only, because in this direction a meaningful fit was obtained. The minima of phase is found to occur at ~ 21 h, which reveals upward propagation with a phase difference of ~ 2.9 h, resulting in a vertical phase velocity of 2.4 km/h. This suggests the 10.9 h wave to have ~ 26.2 km vertical wavelength.

The 12 and 13 April 2010 data show horizontal wavelengths of dominant 7.1 h wave in zonal and meridional directions to be ~ 746 and ~ 1250 km, whereas the vertical wavelength is calculated to be ~ 28.2 km. The horizontal wavelengths in the 19 and 20 April 2010 data are calculated to be ~ 1200 and ~ 900 km in zonal and meridional directions respectively, whereas the vertical wavelength is found to be ~ 38 km. These results are summarized in Table 1.

It is important to state that the study of horizontal wave structures and their propagation has been mostly limited to the intensity data obtained by the optical airglow imaging. The maximum horizontal wavelength that has been monitored with optical imaging and reported in the literature is less than 100 km (refs 13, 15, 20–23). This is primarily due to the limitation of imaging data, where the horizontal wavelengths are estimated using single images and hence large-scale structures cannot be evaluated. The present results report these structures in temperature fields and very large horizontal wavelengths to persist in the data, which may be due to large scanning steps. Possibly, smaller scanning steps at every 5° zenith angle (limited by full field-of-view of the instrument) may provide important insights into the spectrum of temperature waves. Although shorter period waves also exist in the data, we have not derived their scales because our aim is to show large temperature gradients and scales of dominant waves during a single night. Relevant to note is that there had been a few scanning photometer measurements (similar to the one used in the present study) made in the past[24,25], which reported similar (~ 500–4000 km) wavelengths as noted in the present study. It is believed that such temperature measurements are of importance as they provide simultaneous temperature and intensity perturbations[26] together with an estimate of the wavelengths of the perturbations which are required in understanding the coupling studies[5].

Temperature gradient variability

The static and dynamic stability of the atmosphere depends on the temperature gradients. The frequency of natural oscillation of an air parcel depends on the temperature gradient. Further, the vertical propagation of any wave perturbation depends on the frequency of natural oscillation[27,28]. There have been several reports suggesting temperature gradient to be responsible for the observed wave ducting[7,8]. Till date, most of the studies use either Rayleigh lidar or space-borne measurements to derive and utilize the thermal gradients[29,30]. The space-borne methods provide a snapshot information on the thermal structures, whereas Rayleigh lidar measurements provide good information till 75 km altitude.

The present study proposes the use of simultaneous OH and O_2 temperature measurements to retrieve the temperature gradient and its variation with time resolution better than 6 min. Figure 8 shows the temporal variability in the observed temperature gradients on 12 and 13 April 2010. The gradients in all directions are negative; suggesting the mesopause to occur above 94 km. Variation of temperature gradient from one direction to another is an important issue, suggesting the role of short-scale wave features having their scales less than 300 km. The gradient between 87 and 94 km varies from –4 to –8 K/km. As discussed earlier, the SABER pass was available at 13.2°N, 74.8°E (comparable with 65°E data) and 15.6°N, 75.8°E (comparable with northeast data) at 20 : 51 and 20 : 52 IST. The SABER passes show the thermal gradient to be ~ –5 to –6 K/km at 20 : 51 h IST, which agrees well with the obtained value of –5 to –7 K/km shown in Figure 8. Thus, the MLTP measurements compare well with the SABER measurements, which implies that the obtained temperature gradient variability represents true variations in the thermal gradient at upper mesospheric altitudes.

Nocturnal variability of temperature gradient noted on 15 and 16 April 2010 is shown in Figure 3, which needs to be discussed here in detail. In Figure 3, short-period variations in the obtained gradient in all the directions were evident which were further characterized by the LSP analysis. During this night, the temperature gradient is found to be negative, which indicates that the mesopause occurred above 94 km, except at ~ 22 : 30 and 24 : 45 h IST in the 65° east and north scans. Also, SABER passes were available at around 20 : 04 h IST (shown in Figure 7), while the observations started from 20 : 10 h IST. The temperature gradient noted in SABER data varies from –3 to –6 K/km, which compares well with the gradient estimates of –2 to –4 K/km (Figure 3). It can be said that the temperature values as well as the temperature gradient values obtained with SABER and MLTP have close correspondence.

Figure 9 plots the estimated temperature gradient on 19 and 20 April 2010. Similar to the other nights, short-period wave features are noteworthy in the variability and were characterized using the LSP analysis. Except for the zenith measurements, plots reveal the temperature gradient to remain negative throughout the night. After 21 h IST, the gradient at the zenith becomes positive,

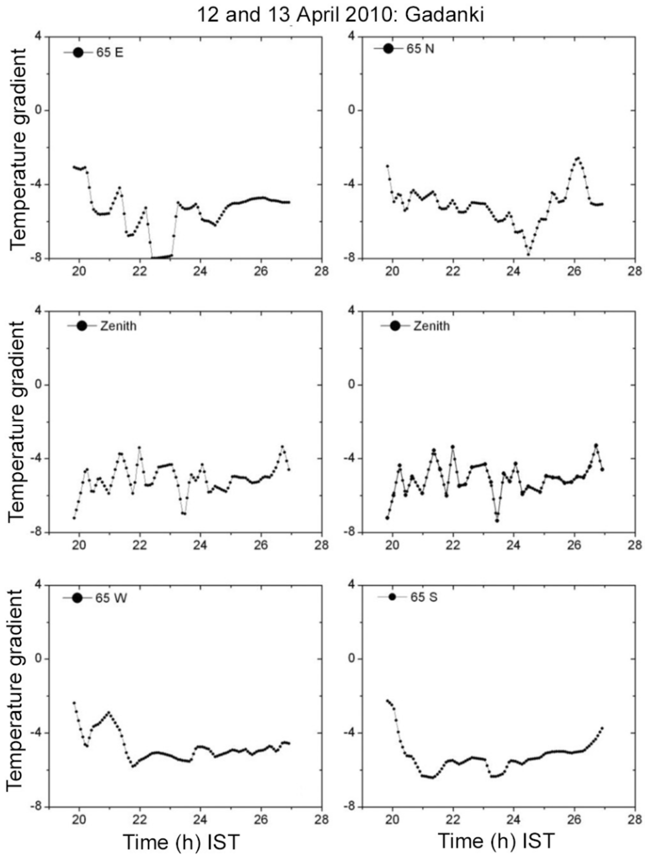

Figure 8. Spatial and temporal variability in the deduced temperature gradient on 12 and 13 April 2010. Rapid variations in the timescales < 15 min are noteworthy.

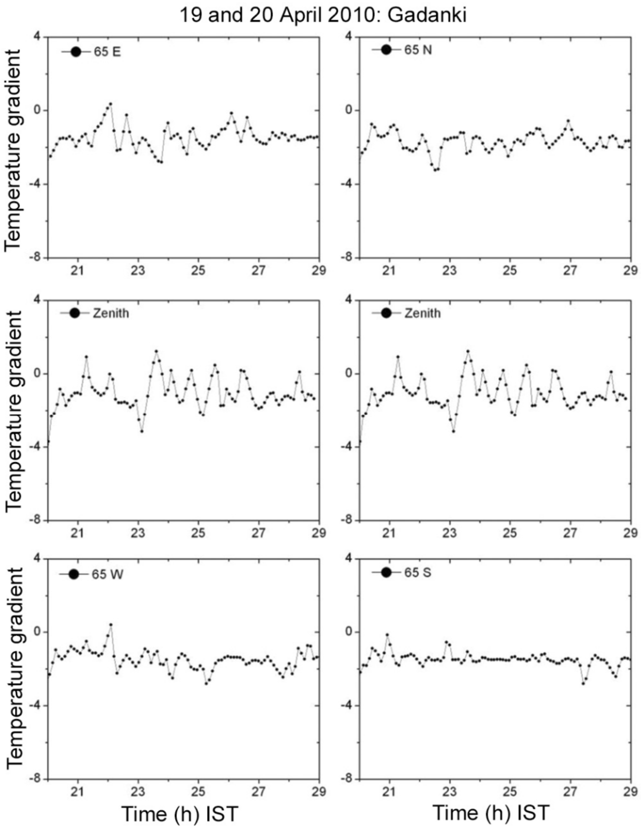

Figure 9. Same as Figure 8, but for 19 and 20 April 2010.

suggesting OH layer to be hotter than O_2 layer for a few minutes. Further positive gradients are noted to occur at ~23 : 50 h, 24 : 45 h, 01 : 30 (25 : 30) h, 02 : 30 (26 : 30) h and 04 : 00 (28 : 00) h IST at the zenith. This suggests large variations in the thermal gradient and the occurrence of multiple temperature inversion layers within 80–100 km. This is supported by the SABER data observed after midnight (Figure 7), where the occurrence of multiple thermal inversions is clearly noted. The temperature gradient in SABER data is found to vary from –4 to –1 K/km, while the MLTP estimates show these values to vary from –4 to 1 K/km. The cause of this difference may be attributed to the occurrence of multiple temperature inversion layers and large variations within 5° latitude–longitude.

With the above discussions, it is suggested that the temperature gradient deduced with simultaneous OH and O_2 data is a good proxy of the layer-averaged background temperature gradient. The only limitation of this method is that it assumes the OH and O_2 layers to be at fixed altitudes, which may not always be true. But, because both emissions depend on the ozone and oxygen profiles and these layers have ~ 8 km layer thickness[31], the effects of altitude variations may not be significant in terms of the layer separation[32]. This aspect needs to be verified by suitable photochemical modelling studies. Important to note is that the mesospheric thermal inversion layers may have short-period variability (as shown in the present study), which is not yet well understood owing to the unavailability of data with high temporal resolution. The present study proposes to use the simultaneous OH and O_2 data to understand the variability associated with them. Further, the short-time period variability in the thermal gradients would alter the frequency of natural oscillation in the upper mesospheric altitudes which has a profound impact on the upward wave propagation through thermal ducting. With initial studies exhibiting short-period variations in thermal gradient, the present study shows the possible usefulness of these data for studying such processes with the help of airglow monitoring.

Conclusions

The salient features of present study are as follows.

1. The nocturnal waves in the data show their zonal and vertical wavelengths to vary from 740 to 4500 km and 26 to 38 km respectively, while their periods were found to vary from 4.1 to 10.3 h.
2. The ground-based OH and O_2 temperature estimates and the deduced temperature gradients are in a reasonable agreement with space-borne SABER measured values.
3. The temperature gradient shows large variations in the temporal scale (from –6 to 1 K/km) as well in the spatial scales, varying from zenith to 65° zenith angles in zonal and meridional directions.

An extended study based on a larger database may provide further insight into the thermodynamical processes and their short-period variability occurring in the upper mesospheric altitudes.

1. Smith, A. K., Global dynamics of the MLT. *Surv. Geophys.*, 2012, **33**, 1281–1334; doi: 10.1007/s10712-012-9196-92012.
2. Fritts, D. C. and Alexander, M. J., Gravity wave dynamics and effects in the middle atmosphere. *Rev. Geophys*., 2003, **41**, 1003; doi: 10.1029/2001RG000106.
3. Aveiro, H. C., Denardini, C. M. and Abdu, M. A., Climatology of gravity waves-induced electric fields in the equatorial E region. *J. Geophys. Res.*, 2009, **114**, A11308; doi: 10.1029/2009JA014177.
4. Makela, J. J. and Otsuka, Y., Overview of nighttime ionospheric instabilities at low- and mid-latitudes: coupling aspects resulting in structuring at the mesoscale. *Space Sci. Rev*., 2011, **168**, 419–440; doi: 10.1007/s11214-011-9816-6.
5. Taori, A., Makela, J. and Taylor, M., Mesospheric wave signatures and equatorial plasma bubbles: a case study. *J. Geophys. Res.*, 2010, **115**; doi: 10.1029/2009JA015088.
6. Taori, A., Patra, A. K. and Joshi, L. M., Gravity wave seeding of equatorial plasma bubbles: an investigation with simultaneous F-region, E-region and middle atmospheric measurements. *J. Geophys. Res.*, 2011, **116**; doi: 10.1029/2010JA016229.
7. Laughman, B., Fritts, D. C. and Werne, J., Numerical simulation of bore generation and morphology in thermal and Doppler ducts. *Ann. Geophys.*, 2009, **27**, 511–523; doi: 10.5194/angeo-27-511-2009.

8. Bageston, J. V., Wrasse, C. M., Batista, P. P., Hibbins, R. E., Fritts, D. C., Gobbi, D. and Andrioli, V. F., Observation of a mesospheric front in a thermal-Doppler duct over King George Island, Antarctica. *Atmos. Chem. Phys.*, 2011, **11**, 12137–12147; doi: 10.5194/acp-11-12137-2011.
9. Sarkhel, S., Raizada, S., Mathews, J. D., Smith, S. M., Tepley, C. A. Rivera, F. J. and Gonzalez, S. A., Identification of large scale billow-like structure in the neutral sodium layer over Arecibo. *J. Geophys. Res.*, 2012; doi: 10.1029/2012JA017891.
10. Collins, R. L., Lehmacher, G. A., Larsen, M. F. and Mizutani, K., Estimates of vertical eddy diffusivity in the upper mesosphere in the presence of a mesospheric inversion layer. *Ann. Geophys.*, 2011, **29**, 2019–2029; doi: 10.5194/angeo-29-2019-2011.
11. Friedman, J. S., Tepley, C. A., Raizada, S., Zhou, Q. H., Hedin, J. and Delgado, R., Potassium Doppler-resonance lidar for the study of the mesosphere and lower thermosphere at the Arecibo Observatory. *J. Atmos. Sol.-Terr. Phys.*, 2003, **65**, 1411–1424.
12. Parihar, N., Taori, A., Gurubaran, S. and Mukherjee, G. K., Simultaneous measurement of OI 557.7 nm, O_2 (0, 1) atmospheric band and OH (6, 2) Meinel band nightglow at Kolhapur (17°N), India. *Ann. Geophys.*, 2013, **31**, 197–208; doi: 10.5194/angeo-31-197-2013.
13. Parihar, A., Taori, A., Kamalakar, V. and Rao, S. V. B., A case study of mesospheric wave periods and horizontal structures over a low latitude station, Allahabad (India). *Earth Sci. Res.*, 2013, **2**, 1; doi: 10.5539/esr.v2n1p1.
14. Scheer, J. and Reisin, E. R., Rotational temperatures for OH and O_2 airglow bands measured simultaneously from El Leoncito (31°48′S). *J. Atmos. Terr. Phys.*, 1990, **52**, 47–57.
15. Taylor, M., Pendleton Jr, W. R., Clark, S., Takahashi, H., Gobbi, D. and Goldberg, R. A., Image measurements of short-period gravity waves at equatorial latitudes. *J. Geophys. Res. D*, 1997, **102**(22), 26283–26299.
16. Takahashi, H., Sahai, Y. and Batista, P. P., Airglow O_2 ($^1\Sigma$) atmospheric band at 8645 Å and the rotational temperature observed at 23°S. *Planet. Space Sci.*, 1986, **34**(3), 301–306.
17. Taori, A., Dashora, N., Raghunath, K., Rusell III, J. M. and Mlynczak, M. G., Simultaneous mesosphere, thermosphere–ionosphere parameter measurements over Gadanki (13.5°N, 79.2°E) – first results. *J. Geophys. Res.*, 2011, **116**; doi: 10.1029/2010JA016154.
18. Remsberg, E. E. *et al.*, Assessment of the quality of the version 1.07 temperature-versus-pressure profiles of the middle atmosphere from TIMED/SABER. *J. Geophys. Res.*, 2008, **113**, D17101; doi: 10.1029/2008JD010013.
19. Taori, A., Taylor, M. and Franke, S., Detection and measurement of a terdiurnal wave signature in the upper mesospheric temperature and wind fields at low latitudes (20°N). *J. Geophys. Res.*, 2005, **110**; doi: 10.1029/2004JD004564.
20. Li, Q., Xu, J., Yue, J., Yuan, W. and Liu, X., Statistical characteristics of gravity wave activities observed by an OH airglow imager at Xinglong, in northern China. *Ann. Geophys.*, 2011, **29**, 1401–1410; doi: 10.5194/angeo-29-1401-2011.
21. Mukherjee, G. K., The signature of short-period gravity waves imaged in the OI 557.7 nm and near infrared OH nightglow emissions over Panhala. *J. Atmos. Sol.-Terr. Phys.*, 2003, **65**, 1329–1335.
22. Suzuki, S., Tsutsumi, M., Palo, S. E., Ebihara, Y., Taguchi, M. and Ejiri, M., Short-period gravity waves and ripples in the South Pole mesosphere. *J. Geophys. Res.*, 2011, **116**, D19109; doi: 10.1029/2011JD015882.
23. Takahashi, H. *et al.*, Simultaneous observation of ionospheric plasma bubbles and mesospheric gravity waves during the SpreadFEx campaign. *Ann. Geophys.*, 2009, **27**, 1477–1487; doi: 10.5194/angeo-27-1477-2009.
24. Elphinstone, R. D., Cogger, L. L., Murphee, J. S., Murty, G. S. N. and Meriwether Jr, J. W., The analysis of hydroxyl rotational temperatures to characterize moving thermal structure near the mesopause. *J. Atmos. Terr. Phys.*, 1988, **50**, 657–668.
25. Takahashi, H., Batista, P. P., Buriti, R. A., Gobbi, D., Nakamura, T., Tsuda, T. and Fukao, S., Simultaneous measurements of airglow OH emission and meteor wind by a scanning photometer and the MU radar. *J. Atmos. Sol. Terr. Phys.*, 1998, **60**, 1649–1668.
26. Taori, A. and Taylor, M., Characteristics of wave induced oscillations in mesospheric O_2 emission intensity and temperatures. *Geophys. Res. Lett.*, 2006, **33**, L01813; doi:1029/2005GL024442.
27. Chimonas, G. and Hines, C. O., Doppler ducting of atmospheric gravity-waves. *J. Geophys. Res.*, 1986, **91**, 1219–1230.
28. Yu, Y. and Hickey, M. P., Numerical modeling of a gravity wave packet ducted by the thermal structure of the atmosphere. *J. Geophys. Res.*, 2007, **112**, A06308; doi: 10.1029/2006JA012092.
29. Sivakumar, V. *et al.*, Lidar measurements of mesospheric temperature inversion at a low latitude. *Annu. Geophys*., 2001, **19**, 1039–1044.
30. Yue, J., She, C.-Y. and Liu, H.-L., Large wind shears and stabilities in the mesopause region observed by Na wind-temperature lidar at midlatitude. *J. Geophys. Res.*, 2010, **115**, A10307; doi: 10.1029/2009JA014864.
31. Takahashi, H. *et al.*, Rocket measurements of the equatorial airglow: MULTIFOT 92 database. *J. Atmos. Terr. Phys.*, 1996, **58**(16), 1943–1961.
32. Nee, J.-B. *et al.*, OH airglow and equatorial variations observed by ISUAL instrument on-board the FORMOSAT 2 satellite. *Terr. Atmos. Ocean. Sci.*, 2010, **21**(6), 985–995; doi: 10.3319/TAO.2010.03.12.01(AA).

ACKNOWLEDGEMENTS. We thank V. Kamalakar and Liyakat Basha for help while carrying out night airglow measurements, and the Director, National Atmospheric Research Laboratory, Gadanki for encouragement.

Received 10 October 2013; revised accepted 5 December 2013